FELDER, S, and CHANSON, H. (2012). "Free-surface Profiles, Velocity and Pressure Distributions on a Broad-Crested Weir: a Physical study." *Journal of Irrigation and Drainage Engineering*, ASCE, Vol. 138, No. 12, pp. 1068–1074 (DOI: 10.1061/(ASCE)IR.1943-4774.0000515) (ISSN 0733-9437).

FREE-SURFACE PROFILES, VELOCITY AND PRESSURE DISTRIBUTIONS ON A BROAD-CRESTED WEIR: A PHYSICAL STUDY

by Stefan FELDER[1] and Hubert CHANSON[2]

Abstract: Basic experiments were conducted on a large-size broad-crested weir with a rounded corner. Detailed free-surface, velocity and pressure measurements were performed for a range of flow conditions. The results showed the rapid flow distribution at the upstream end of the weir, as well as next to the weir brink at large flow rates. The flow properties above the crest were analysed taking into account the non-uniform velocity and non-hydrostatic pressure distributions. Introducing some velocity and pressure correction coefficients, it is shown that critical flow conditions were achieved above the weir crest for $0.1 < x/L_{crest} < 1$. The velocity measurements highlighted a developing boundary layer. The data differed from the smooth turbulent boundary layer theory, although the present results were consistent with earlier studies. On average the boundary stress was about $\tau_o/(\rho \times g \times H_1) \sim 0.0015$ to 0.0025.

Keywords: broad-crested weir, free-surface profile, velocity distributions, pressure distributions, critical flow conditions, turbulent boundary layer.

INTRODUCTION

A broad-crested weir is a flat-crested structure with a length L_{crest} large compared to the flow thickness (HARRISON 1967, MONTES 1969) (Fig. 1). The crest is termed broad when the flow streamlines are parallel to the crest and the pressure distribution is hydrostatic (BOS 1976, MONTES 1998). The discharge above the weir may be estimated as:

$$Q = C_D \times \sqrt{g \times \left(\frac{2}{3} \times H_1\right)^3} \times B \qquad (1)$$

where Q is the flow rate, B is the channel breadth, g is the gravity acceleration, H_1 is the upstream total head above crest (Fig. 1), and C_D is a dimensionless discharge coefficient (HENDERSON 1966, CHANSON 2004).

[1] Ph.D. student, School of Civil Engineering, The University of Queensland, Brisbane QLD 4072, Australia

[2] Professor in Hydraulic Engineering, School of Civil Engineering, The University of Queensland, Brisbane QLD 4072, Australia. Email: h.chanson@uq.edu.au.

The hydraulic characteristics of broad-crested weirs were studied during the 19th and 20th centuries. BÉLANGER (1841,1849) analysed theoretically the overflow and he derived Equation (1) for the ideal case (C_D = 1). Successful physical studies included BAZIN (1896), WOODBURN (1932), TISON (1950) and SERRE (1953). HALL (1962) and ISAACS (1981) studied the effects of developing boundary layer on the overflow. RAMAMURTHY et al. (1988) investigated systematically the discharge characteristics of round-edged and square-edged weirs and SARGISON and PERCY (2009) showed the influence of the weir inflow design on the bottom pressure distributions and discharge coefficient. GONZALEZ and CHANSON (2007) studying the flow above a large weir highlighted the impact of large vortical structures observed immediately upstream of the weir.

It is the purpose of this contribution to document the free-surface profiles and pressure and velocity distributions on a horizontal broad-crested weir with rounded nose. New experiments were performed in a large size facility. The results provide new insights into the vertical profiles of pressure and velocity on the broad-crest, including the boundary layer development and salient flow patterns.

EXPERIMENTAL APPARATUS

New experiments were conducted at the University of Queensland in a 7 m long, 0.52 m wide test section. Waters were supplied from a large 1.5 m deep feeding basin with a surface area of 2.9 m × 2.2 m leading to a sidewall convergent (1.01 m long) with a 4.23:1 contraction ratio enabling an very smooth and waveless inflow. The weir consisted of a 1 m high, 0.52 m wide and 1.01 m long flat horizontal crest with an upstream rounded corner (0.080 m radius). The crest was made of smooth painted marine ply. Additional measurements were carried out in a 0.25 m wide glass channel (Table 1).

A pump controlled with an adjustable frequency AC motor drive delivered the flow rate, enabling an accurate discharge adjustment in a closed-circuit system. Clear-water flow depths were measured on the channel centreline with a point gauge and using photographs through the sidewalls. Sidewall photography was undertaken with dSLR cameras, Canon™ EOS 450D and Pentax™ K-7, and the lens distortion correction was performed with the software PTLens™ v. 8.7.8. The point gauge and photographic data yielded the same results within 0.5 mm. Pressure and velocity measurements were performed with a Prandtl-Pitot tube (Ø = 3.0 mm). The tube was connected to an inclined manometer which gave both total and piezometric heads. The translation of the Pitot-Prandtl probe in the vertical direction was controlled by a fine adjustment travelling mechanism. The error on the vertical position of the probe was less than 0.25 mm. The accuracy on the longitudinal position was estimated as $\Delta x <$ +/- 1 mm. The accuracy on the transverse position of the probe was less than 1 mm.

BASIC FLOW PATTERNS

The inflow conditions were quiescent for all investigated flow conditions. The free-surface upstream of and above the crest was very smooth. Immediately upstream of the weir crest, the flow accelerated, was critical above the crest and became supercritical on the downstream steep slope (Fig. 1). Next to the upstream end of the crest, the flow was rapidly varied and characterised by some free-surface curvature (Fig. 2) and some rapid change in pressure and velocity distributions. Figure 2 presents some typical free-surface profiles recorded above the crest. The data highlighted that the free-surface profile above the weir crest is not horizontal as previously reported (WOODBURN 1932, HARRISON 1967). For some flow conditions, some wavy profile was observed above the crest: for example, for H_1/L_{crest} = 0.06 and 0.10 in Figure 2. These might be linked with the interactions of the developing boundary layer with the main flow as discussed by ISAACS (1981).

Above the broad crest, the specific energy was minimum and critical flow conditions took place. Although the water surface was not horizontal, the depth-averaged specific energy was basically constant above the entire crest. Herein the depth-averaged specific energy above the crest is commonly expressed following LIGGETT (1993) and CHANSON (2006) as:

$$H = \frac{\int_0^d \left(\frac{v_x{}^2}{2 \times g} + z + \frac{P}{\rho \times g} \right) \times dy}{d} = \beta \times \frac{V^2}{2 \times g} + \Lambda \times d \quad (2)$$

where H is the depth-averaged specific energy, d is the flow depth, P is the pressure, V is the depth-averaged velocity, y is the vertical elevation above the crest, β is the momentum correction coefficient or Boussinesq coefficient, and Λ is the pressure correction coefficient defined as:

$$\Lambda = \frac{1}{2} + \frac{1}{d} \times \int_0^d \frac{P}{\rho \times g \times d} \times dy \quad (3)$$

For an uniform flow above a flat broad crest with the streamlines parallel to the crest, the velocity distribution is uniform (β = 1), the pressure is hydrostatic (Λ = 1), and Equation (2) equals the classical result:

$$H = \frac{V^2}{2 \times g} + d = \frac{3}{2} \times \sqrt[3]{\frac{Q^2}{g \times B^2}} \quad (4)$$

In practice, however, the velocity distributions were not uniform along the crest because of the bed friction above the crest and a turbulent boundary layer develops. Further the streamlines and free-surface were not parallel to the crest everywhere (Fig. 2).

When the specific energy is minimum, the flow depth above the crest is critical (BAKHMETEFF 1932, HENDERSON 1966) and must satisfy one of the four physical solutions (CHANSON 2006):

$$\frac{d}{H} \times \Lambda = \sqrt[3]{\frac{1 - 2 \times \beta \times {C_D}^2 \times \Lambda^2}{27} + \Lambda^3 \times \sqrt{\Delta}} + \sqrt[3]{\frac{1 - 2 \times \beta \times {C_D}^2 \times \Lambda^2}{27} - \Lambda^3 \times \sqrt{\Delta}} + \frac{1}{3} \qquad \Delta > 0 \text{ (5a)}$$

$$\frac{d}{H} \times \Lambda = \frac{2}{3} \qquad \Delta = 0 \text{ (5b)}$$

$$\frac{d}{H} \times \Lambda = \frac{2}{3} \times \left(\frac{1}{2} + \cos\frac{\varepsilon}{3} \right) \qquad \Delta < 0 \text{ \& Solution S1 (5c)}$$

$$\frac{d}{H} \times \Lambda = \frac{2}{3} \times \frac{1 - \cos\frac{\varepsilon}{3} + \sqrt{3 \times \left(1 - \left(\cos\frac{\varepsilon}{3} \right)^2 \right)}}{2} \qquad \Delta < 0 \text{ \& Solution S3 (5d)}$$

where:

$$\cos\varepsilon = 1 - 2 \times \beta \times {C_D}^2 \times \Lambda^2 \qquad (6)$$

and the discriminant Δ equals:

$$\Delta = \frac{4 \times \beta \times {C_D}^2 \times \Lambda^2}{(3 \times \Lambda)^6} \times (\beta \times {C_D}^2 \times \Lambda^2 - 1) \qquad (7)$$

Equation (5) expresses the flow depth at critical flow conditions in the general case when $\beta > 1$ and $\Lambda \neq 1$. Present experimental data were tested against Equation (5). Typical results are presented in Figure 3 in terms of the dimensionless water depth $d \times \Lambda / H_1$ as a function of $\beta \times {C_D}^2 \times \Lambda^2$, where β, C_D and Λ were calculated based upon the pressure and velocity distribution data. The whole data set is also reported in Appendix. C_D was estimated using Equation (1) in which the discharge per unit width was deduced from the equation of conservation of mass:

$$\frac{Q}{B} = \int_0^d v_x \times dy \qquad (8)$$

In Figure 3, each data set regroups the flow depth measurements for $0.1 < x/L_{crest} < 1$, and they are compared with experimental results obtained above circular crested weirs (FAWER 1937, VO 1992) and in undular flows (CHANSON 2005). The present results showed overall a reasonable agreement between data and theory, in particular the solutions S1 and S3 ($\Delta < 0$), along the entire weir crest (Fig. 3). The agreement between Equation (5) and data highlighted that the assumption of critical flow conditions holds along the crest ($0.1 < x/L_{crest} < 1$) despite the boundary layer development and the non-horizontal free-surface.

Note that the flow depth above the crest differed from the classical expression $\sqrt[3]{Q^2/(g \times B^2)}$ because of the non-uniform velocity and non-hydrostatic pressure distributions.

VELOCITY AND PRESSURE DISTRIBUTIONS

The vertical distributions of velocity and pressure were measured along the crest for a range of flow conditions ($0.02 < H_1/L_{crest} < 0.3$). The experimental data showed systematically the redistributions of pressure and velocity profiles at the upstream and downstream ends of the broad crest (Fig. 4). For $x/L_{crest} < 0.2$, the pressure gradient was typically less hydrostatic, and the velocity profile had a shape close to that predicted by ideal-fluid flow theory and flow net considerations. At the downstream end, the free-surface curvature became pronounced as the flow accelerated near the brink (Fig. 2). At the brink, the velocity and pressure profiles were similar to those observed at a free overfall (HENDERSON 1966) (Fig. 4). Some typical velocity and pressure distribution data are shown in Figure 4 and the figure captions detail the flow conditions. Figures 4A and 4B present some dimensionless velocity profiles for two dimensionless heads above crest. Note that the velocity data at $x/L_{crest} = -0.065$ upstream of the crest were the longitudinal velocity component data only. Figure 4C shows the dimensionless pressure distributions for the experiment presented in Figure 4B; the solid line (slope 1:1) is the hydrostatic pressure distribution. In Figure 4C the pressure distributions at $x/L_{crest} = 0.11$ & 0.78 differ from the hydrostatic profile and they are compared with an inviscid solution of the Boussinesq equation (MONTES and CHANSON 1998) which was calculated based upon the measured free-surface slope and curvature. Although the effect of boundary friction could be included (CASTRO-ORGUAZ and CHANSON 2011), it is believed that the observed non-hydrostatic pressure distribution resulted primarily from an inviscid velocity redistribution rather than from boundary friction effects.

The rapid flow redistribution at the upstream end of the weir crest was associated with the development of a turbulent boundary layer. At the upstream end of the crest, the flow was essentially irrotational, but the no-slip condition at the crest invert (y = 0) induced a boundary layer growth. The boundary layer development was estimated from the measured velocity profiles. Results are presented in Figure 5 where they are compared with the boundary layer growth above a smooth flat plate in absence of pressure gradient for two flow conditions. For the present data, the boundary layer thickness development was best correlated by:

$$\frac{\delta}{x} \sim \left(\frac{x}{k_s}\right)^{-0.124} \qquad x/L_{crest} < 0.7 \quad (9)$$

where δ is the boundary layer thickness defined in terms of 99% of the free-stream velocity and k_S is the equivalent sand roughness height (herein $k_S = 0.5$ mm). The boundary layer growth was about $\delta \sim$

$x^{0.87}$ compared to a smooth turbulent boundary layer growth of $\delta \sim x^{0.8}$ (SCHLICHTING 1979, CHANSON 2009). Note that the free-surface data implied indeed a slight favourable longitudinal pressure gradient, and it is acknowledged that the comparison with the zero pressure gradient boundary layer theory might have some limitation.

The boundary layer data showed further an apparent reduction in boundary layer thickness at the downstream end of the crest for the larger discharges: i.e., $H_1/L_{crest} > 0.18$. This is highlighted in Figure 5 (symbols with arrow on right). It is believed to be caused by some velocity redistributions induced by the free-surface and streamline curvature of the flow. A similar flow redistribution at the crest downstream end was documented by VIERHOUT (1973) and MATOS (2011, Pers. Comm.).

DISCUSSION

In a smooth turbulent boundary layer, the solution of Prandlt's mixing length yields the law of the wall characterising the velocity profile in the inner flow region:

$$\frac{v_x}{V_*} = 2.5 \times \text{Ln}\left(\frac{\rho \times V_* \times y}{\mu}\right) + 5 \qquad y/\delta < 0.15 \quad (10)$$

where V_* is the shear velocity ($V_* = \sqrt{\tau_o / \rho}$), μ is the dynamic viscosity and τ_o is the boundary shear stress (SCHLICHTING 1979, MONTES 1998). The boundary shear stress over the crest was estimated from the velocity measurements in the developing boundary layer by the best fit of the data with Equation (10) in the inner region. The results were compared with the boundary shear stress calculated from the von Karman momentum integral equation:

$$\frac{\tau_o}{\rho} = \frac{\partial}{\partial x}(U^2 \times \delta_2) + U \times \delta_1 \times \frac{\partial U}{\partial x} \qquad (11)$$

where U is the free-stream velocity: $U = v_x(y>\delta)$, and δ_1 and δ_2 are respectively the displacement and momentum thicknesses (LIGGETT 1994, CHANSON 2009). The boundary shear stress data are presented in Figure 6: both results derived from Equations (10) and (11) are presented and compared with the data VIERHOUT (1973) obtained using a Preston tube. Despite some scatter, the data yielded a dimensionless boundary shear stress $\tau_o/(\rho \times g \times H_1) = 0.0015$ and 0.0025 on average using Equations (10) and (11) respectively, while the data of VIERHOUT gave $\tau_o/(\rho \times g \times H_1) = 0.0016$ on average.

The discharge per unit width was calculated from the integration of the measured velocity profiles (Eq. (8)) on the middle of the crest ($x/L_{crest} = 0.55$). The data are summarised in Figure 7 in terms of the dimensionless discharge coefficient C_D (Eq. (1)) and they are compared with previous studies of broad-crested weirs obtained with upstream rounded edge (BAZIN 1896, VIERHOUT 1973, GONZALEZ and CHANSON 2007), square edge (BAZIN 1896, SARGISON and PERCY 2009) and inclined upstream wall (SARGISON and PERCY 2009) (Table 1). Figure 7 illustrates the lower

discharge capacity of square edged weirs linked with the adverse role of the upstream separation bubble (MOS 1972).

The present results showed a slight increase in discharge coefficient with increasing head above crest similar to previous studies. For large dimensionless heads above crest, the weir would no longer act as broad-crest, and the discharge coefficient would tend to values close to those observed on rounded weirs (circular, ogee). Overall the dimensionless discharge coefficient data was best correlated by:

$$C_D = 0.92 + 0.153 \times \frac{H_1}{L_{crest}} \qquad \text{Large weir } (\Delta z = 1.0 \text{ m}) \quad (12)$$

for $0.02 < H_1/L_{crest} < 0.3$. Equation (12) is shown in Figure 7.

The present data trend differed from the data of GONZALEZ and CHANSON (2007) who observed the occurrence of irregular corner eddies next to the sidewalls immediately upstream of the vertical upstream wall, associated with instabilities affecting the overflow motion. In the present study, the inflow conditions were very smooth and no irregular vortice generation was observed.

CONCLUSION

Some basic experiments were conducted on a large broad-crested weir with rounded corner. Both free-surface profiles and pressure and velocity distributions were recorded for a relatively wide range of flow conditions ($0.02 < H_1/L_{crest} < 0.3$).

The results highlighted the rapid redistributions of velocity and pressure fields at the upstream and downstream ends of the crest although the flow was critical along the crest (Fig. 3). This was rarely documented in a large facility under controlled flow conditions. At the upstream end, the flow motion was irrotational and the pressure and velocity distributions were affected by the streamline and free-surface curvature. At the downstream end of the crest, the flow properties were close to those observed at the brink of an overfall. The velocity distributions measurements highlighted a developing boundary layer. While the data differed from the smooth turbulent boundary layer theory, the results were consistent with earlier studies. The dimensionless boundary stress was on average $\tau_o/(\rho \times g \times H_1) \sim 0.0015$ to 0.0025 and the result was nearly independently of the measurement technique: namely using the best fit to the log-law and the momentum integral equation. A correlation was derived for the dimensionless discharge coefficient C_D that was close to earlier results with rounded broad crests and C_D was typically larger than for square broad crests (Fig. 7).

FELDER, S, and CHANSON, H. (2012). "Free-surface Profiles, Velocity and Pressure Distributions on a Broad-Crested Weir: a Physical study." *Journal of Irrigation and Drainage Engineering*, ASCE, Vol. 138, No. 12, pp. 1068–1074 (DOI: 10.1061/(ASCE)IR.1943-4774.0000515) (ISSN 0733-9437).

ACKNOWLEDGMENTS

The writers thank Ahmed IBRAHIM and Jason VAN DER GEVEL (The University of Queensland) for the technical assistance. The financial support of the Australian Research Council (Grant DP0878922) is acknowledged. The first author was supported by an University of Queensland research scholarship.

APPENDIX - EXPERIMENTAL INVESTIGATIONS OF PRESSURE AND VELOCITY DISTRIBUTIONS IN CRITICAL FLOW CONDITIONS

Run.	H_1 m	H_1/L_{crest}	x/L_{crest}	C_D	β	Λ	$\beta \times C_D^2 \times \Lambda^2$	$\Lambda \times d/H_1$
(1)	(2)	(3)	(4)	(5)	(6)	(7)	(8)	(9)
60mm	0.06	0.059	0.11	1.000	0.959	0.986	0.931	0.780
60mm	0.06	0.059	0.23	0.993	1.012	0.949	0.899	0.767
60mm	0.06	0.059	0.34	0.968	1.012	0.948	0.852	0.743
60mm	0.06	0.059	0.44	0.971	1.015	0.931	0.830	0.714
60mm	0.06	0.059	0.55	0.927	1.015	0.996	0.865	0.697
60mm	0.06	0.059	0.78	0.925	1.020	1.001	0.875	0.668
60mm	0.06	0.059	1.00	0.997	1.029	0.362	0.134	0.157
100mm	0.1	0.099	0.11	0.920	1.006	1.001	0.853	0.786
100mm	0.1	0.099	0.23	0.948	1.009	1.019	0.941	0.698
100mm	0.1	0.099	0.34	0.974	1.012	0.985	0.931	0.758
100mm	0.1	0.099	0.44	0.961	1.026	0.969	0.890	0.746
100mm	0.1	0.099	0.55	0.962	0.995	1.007	0.934	0.665
100mm	0.1	0.099	0.78	0.950	1.014	0.995	0.906	0.627
100mm	0.1	0.099	1.00	0.983	1.011	0.832	0.677	0.375
140mm	0.14	0.139	0.11	0.947	1.008	1.001	0.906	0.815
140mm	0.14	0.139	0.23	0.954	1.007	1.011	0.938	0.693
140mm	0.14	0.139	0.34	0.950	1.009	1.005	0.920	0.625
140mm	0.14	0.139	0.44	0.935	1.009	1.009	0.898	0.627
140mm	0.14	0.139	0.55	0.932	1.011	1.003	0.885	0.634
140mm	0.14	0.139	0.78	0.924	1.013	1.000	0.864	0.625
140mm	0.14	0.139	1.00	0.971	1.010	0.744	0.527	0.351
180mm	0.18	0.178	0.11	0.988	1.006	0.983	0.947	0.803
180mm	0.18	0.178	0.23	0.960	1.006	1.010	0.946	0.729
180mm	0.18	0.178	0.34	0.966	1.007	1.008	0.956	0.650
180mm	0.18	0.178	0.44	0.962	1.008	1.007	0.946	0.629
180mm	0.18	0.178	0.55	0.949	1.009	1.005	0.916	0.608
180mm	0.18	0.178	0.78	0.943	1.011	0.994	0.889	0.585
180mm	0.18	0.178	1.00	0.973	1.008	0.773	0.570	0.357
220mm	0.22	0.218	0.11	0.957	1.007	0.974	0.875	0.839
220mm	0.22	0.218	0.23	0.956	1.005	1.005	0.928	0.767
220mm	0.22	0.218	0.34	0.962	1.005	1.003	0.934	0.693
220mm	0.22	0.218	0.44	0.957	1.006	1.008	0.936	0.650
220mm	0.22	0.218	0.55	0.950	1.006	1.004	0.915	0.625
220mm	0.22	0.218	0.78	0.932	1.006	0.985	0.848	0.558
220mm	0.22	0.218	1.00	0.974	1.008	0.726	0.504	0.333

260mm	0.26	0.257	0.11	0.952	1.008	0.963	0.847	0.820
260mm	0.26	0.257	0.23	0.951	1.005	0.997	0.905	0.769
260mm	0.26	0.257	0.34	0.945	1.005	0.932	0.780	0.649
260mm	0.26	0.257	0.44	0.945	1.005	1.004	0.904	0.654
260mm	0.26	0.257	0.55	0.943	1.005	0.999	0.893	0.621
260mm	0.26	0.257	0.78	0.954	1.006	0.983	0.884	0.567
260mm	0.26	0.257	1.00	0.970	1.007	0.718	0.488	0.329

NOTATION

The following symbols are used in this paper:

B	channel breadth (m);
C_D	dimensionless discharge coefficient;
d	water depth (m);
g	gravity acceleration (m/s^2);
H	total head (m);
H_1	upstream total head (m) measured above the crest;
k_s	equivalent sand roughness height (m);
L_{crest}	crest length (m) measured in the flow direction;
Q	water discharge (m^3/s);
P	pressure;
R	radius of curvature (m);
U	free-stream velocity (m/s);
V	flow velocity (m/s): V = Q/(d×B);
V_*	shear velocity (m/s);
v_x	longitudinal velocity component (m/s);
x	longitudinal distance (m) measured from the crest upstream end;
y	distance (m) normal to the crest invert;
∅	diameter (m);
β	momentum correction coefficient, also called Boussinesq coefficient;
Δz	weir height (m) above upstream channel invert;
Δ	discriminant;
δ	boundary layer thickness (m);
δ_1	boundary layer displacement thickness (m);
δ_2	boundary layer momentum thickness (m);
ε	dimensionless term;
Λ	pressure correction coefficient;
μ	dynamic viscosity of water (Pa.s);

ρ water density (kg/m^3);

τ_o boundary shear stress (Pa).

REFERENCES

BAKHMETEFF, B.A. (1932). "Hydraulics of Open Channels." *McGraw-Hill*, New York, USA, 1st ed., 329 pages.

BAZIN, H. (1896). "Expériences Nouvelles sur l'Ecoulement par Déversoir." ('Recent Experiments on the Flow of Water over Weirs.') *Mémoires et Documents, Annales des Ponts et Chaussées*, Paris, France, Sér. 7, Vol. 12, 2nd Sem., pp. 645-731 Plates (in French).

BÉLANGER, J.B. (1841). "Notes sur l'Hydraulique." ('Notes on Hydraulic Engineering.') *Ecole Royale des Ponts et Chaussées*, Paris, France, session 1841-1842, 223 pages (in French).

BÉLANGER, J.B. (1849). "Notes sur le Cours d'Hydraulique." ('Notes on the Hydraulics Subject.') *Mém. Ecole Nat. Ponts et Chaussées*, Paris, France (in French).

BOS, M.G. (1976). "Discharge Measurement Structures." *Publication No. 161*, Delft Hydraulic Laboratory, Delft, The Netherlands (also Publication No. 20, ILRI, Wageningen, The Netherlands).

CASTRO-ORGAZ, O, and CHANSON, H. (2011). "Near-Critical Free-Surface Flows: Real Fluid Flow Analysis." *Environmental Fluid Mechanics*, Vol. 11, No. 5, pp. 499-516 (DOI: 10.1007/s10652-010-9192-x).

CHANSON, H. (2004). "The Hydraulics of Open Channel Flows: An Introduction." *Butterworth-Heinemann*, Oxford, UK, 2nd edition, 630 pages.

CHANSON, H. (2005). "Physical Modelling of the Flow Field in an Undular Tidal Bore." *Jl of Hyd. Res.*, IAHR, Vol. 43, No. 3, pp. 234-244.

CHANSON, H. (2006). "Minimum Specific Energy and Critical Flow Conditions in Open Channels." *Journal of Irrigation and Drainage Engineering*, ASCE, Vol. 132, No. 5, pp. 498-502 (DOI: 10.1061/(ASCE)0733-9437(2006)132:5(498)).

CHANSON, H. (2009). "Applied Hydrodynamics: An Introduction to Ideal and Real Fluid Flows." *CRC Press*, Taylor & Francis Group, Leiden, The Netherlands, 478 pages.

FAWER, C. (1937). "Etude de Quelques Ecoulements Permanents à Filets Courbes." ('Study of some Steady Flows with Curved Streamlines.') *Thesis*, Lausanne, Switzerland, Imprimerie La Concorde, 127 pages (in French).

GONZALEZ, C.A., and CHANSON, H. (2007). "Experimental Measurements of Velocity and Pressure Distribution on a Large Broad-Crested Weir." *Flow Measurement and Instrumentation*, Vol. 18, No. 3-4, pp. 107-113 (DOI 10.1016/j.flowmeasinst.2007.05.005).

FELDER, S, and CHANSON, H. (2012). "Free-surface Profiles, Velocity and Pressure Distributions on a Broad-Crested Weir: a Physical study." *Journal of Irrigation and Drainage Engineering*, ASCE, Vol. 138, No. 12, pp. 1068–1074 (DOI: 10.1061/(ASCE)IR.1943-4774.0000515) (ISSN 0733-9437).

HALL, G.W. (1962). "Analytical Determination of the Discharge Characteristics of Broad-Crested Weirs using Boundary Layer Theory." *Proc. Instn. Civ. Engrs.*, London, Vol. 22, June, paper No. 6607, pp. 177-190

HARRISON, A.J.M. (1967). "The Streamlined Broad-Crested Weir." *Proc. Instn. Civil Engrs.*, London, Vol. 38, Dec., pp. 657-678. Discussion: Vol. 42, 1969, Mar., pp. 575-599.

HENDERSON, F.M. (1966). "Open Channel Flow." *MacMillan Company*, New York, USA.

ISAACS, L.T. (1981). "Effects of Laminar Boundary Layer on a Model Broad-Crested Weir." *Research Report No. CE28*, Dept. of Civil Eng., Univ. of Queensland, Brisbane, Australia, 20 pages.

LIGGETT, J.A. (1993). "Critical Depth, Velocity Profiles and Averaging." *Journal of Irrigation and Drainage Engineering*, ASCE, Vol. 119, No. 2, pp. 416-422.

LIGGETT, J.A. (1994). "Fluid Mechanics." *McGraw-Hill*, New York, USA.

MONTES, J.S. (1969). "The Streamlined Broad-Crested Weir. Discussion." *Proc. Instn. Civil Engrs.*, London, Vol. 42, Mar., pp. 576-578.

MONTES, J.S. (1998). "Hydraulics of Open Channel Flow." *ASCE Press*, New-York, USA, 697 pages.

MONTES, J.S., and CHANSON, H. (1998). "Characteristics of Undular Hydraulic Jumps. Results and Calculations." *Journal of Hydraulic Engineering*, ASCE, Vol. 124, No. 2, pp. 192-205.

MOS, W.D. (1972). "Flow Separation at the Upstream Edge of a Square-Edged Broad-crested Weir." *Jl of Fluid Mech.*, Vol. 52, Part 2, pp. 307-320 & 1 plate.

RAMAMURTHY, A.S., TIM, U.S., and RAO, M.V.J. (1988). "Characteristics of Square-Edged and Round-Nosed Broad-Crested Weirs." *Jl of Irrig and Drainage. Engrg.*, ASCE, Vol. 114, No. 1, pp. 61-73.

RAO, N.S. Govinda, and MURALIDHAR, D. (1963). "Discharge Characteristics of Weirs of Finite Crest Width." *Jl La Houille Blanche*, Vol. 18, No. 5, Aug.-Sept., pp. 537-545.

SARGISON, J.E., and PERCY A. (2009). "Hydraulics of Broad-Crested Weirs with Varying Side Slopes." *Jl of Irrigation and Drainage Engrg.*, ASCE, Vol. 135, No. 1, pp. 115-118.

SCHLICHTING, H. (1979). "Boundary Layer Theory." *McGraw-Hill*, New York, USA, 7th edition.

SERRE, F. (1953). "Contribution à l'Etude des Ecoulements Permanents et Variables dans les Canaux." ('Contribution to the Study of Permanent and Non-Permanent Flows in Channels.') *Jl La Houille Blanche*, Dec., pp. 830-872 (in French).

TISON, L.J. (1950). "Le Déversoir Epais." ('Broad-Crested Weir.') *Jl La Houille Blanche*, pp. 426-439 (in French).

VIERHOUT, M.M. (1973). "On the Boundary Layer Development in Round Broad-Crested Weirs with a Rectangular Control section." *Report No. 3*, Lab.Hydraulics and Catchment Hydrology, Agricultural University, Wageningen, The Netherlands, 73 pages.

FELDER, S, and CHANSON, H. (2012). "Free-surface Profiles, Velocity and Pressure Distributions on a Broad-Crested Weir: a Physical study." *Journal of Irrigation and Drainage Engineering*, ASCE, Vol. 138, No. 12, pp. 1068–1074 (DOI: 10.1061/(ASCE)IR.1943-4774.0000515) (ISSN 0733-9437).

VO, N.D. (1992). "Characteristics of Curvilinear Flow Past Circular-Crested Weirs." *Ph.D. thesis*, Concordia Univ., Canada.

WOODBURN, J.G. (1932). "Tests of Broad-Crested Weirs." *Transactions*, ASCE, Vol. 96, pp. 387-416. Discussion: Vol. 96, pp. 417-453.

FELDER, S, and CHANSON, H. (2012). "Free-surface Profiles, Velocity and Pressure Distributions on a Broad-Crested Weir: a Physical study." *Journal of Irrigation and Drainage Engineering*, ASCE, Vol. 138, No. 12, pp. 1068–1074 (DOI: 10.1061/(ASCE)IR.1943-4774.0000515) (ISSN 0733-9437).

LIST OF CAPTIONS

Fig. 1 - Definition sketch of a broad-crested weir

Fig. 2 - Dimensionless free-surface profiles above a broad-crested weir - Both point gauge (small squares & dashed line) and photographic (small crosses) data are presented, and the weir profile is shown in black - Note the distorted scale

Fig. 3 - Dimensionless flow depth above the weir crest $d \times \Lambda / H_1$ as a function of $\beta \times C_D^2 \times \Lambda^2$ - Comparison between broad-crested weir data (Present study, $0.1 < x/L_{crest} < 1$), analytical solutions (Eq. (5)), circular crested weir data (FAWER 1937, VO 1992) and undular flow data (CHANSON 2005)

Fig. 4 - Dimensionless distributions of velocity and pressure along the broad-crested weir
(A) Velocity distributions for $H_1/L_{crest} = 0.139$
(B) Velocity distributions for $H_1/L_{crest} = 0.224$
(C) Pressure distributions for $H_1/L_{crest} = 0.224$ - Comparison with the hydrostatic pressure and a Boussinesq equation solution for $x/L_{crest} = 0.109$ & 0.777

Fig. 5 - Dimensionless boundary layer thickness δ/H_1 - Comparison with the smooth boundary layer theory for $H_1/L_{crest} = 0.099$ & 0.178

Fig. 6 - Dimensionless boundary shear stress $\tau_o/(\rho \times g \times H_1)$ above the crest - Comparison between logarithmic law and momentum integral equation results and the data of VIERHOUT (1973) obtained with a Preston tube

Fig. 7 - Dimensionless discharge coefficients for broad-crested weirs - Comparison with Equation (12), and previous studies with square-edge (BAZIN 1896, SARGISON and PERCY 2009), rounded edge (BAZIN 1896, VIERHOUT 1973, GONZALEZ and CHANSON 2007) and inclined upstream wall (SARGISON and PERCY 2009)

FELDER, S, and CHANSON, H. (2012). "Free-surface Profiles, Velocity and Pressure Distributions on a Broad-Crested Weir: a Physical study." *Journal of Irrigation and Drainage Engineering*, ASCE, Vol. 138, No. 12, pp. 1068–1074 (DOI: 10.1061/(ASCE)IR.1943-4774.0000515) (ISSN 0733-9437).

Table 1 - Experimental investigations of horizontal broad-crested weirs

Experiment	L_{crest} m	Δz m	B m	Q m^3/s	H_1 m	H_1/L_{crest}	Remarks
(1)	(2)	(3)	(4)	(5)	(6)	(7)	(8)
Sharp-edged weir							
BAZIN (1896)	0.40	0.75	2.0	--	0.064 to 0.402	0.159 to 1.0	Sér. 113.
	0.80	0.75	2.0	--	0.062 to 0.42	0.0779 to 0.527	Sér. 114.
	1.99	0.75	2.0	--	0.06 to 0.447	0.03 to 0.225	Sér. 115.
WOODBURN (1932)	3.05	0.533	0.6096	--	0.1524 to 0.457	0.05 to 0.2	
TISON (1950)	1.80	0.30	0.50	0.0073 to 0.041	0.042 to 0.132	0.023 to 0.073	
RAO & MURALIDHAR (1963)	0.10 to 3.0	0.3	0.610	up to 0.14	0.03 to 0.25	0.017 to 1.9	
MOS (1972)	0.15	0.152	0.610	--	0.051 & 0.76	0.336 & 0.5	
	0.381	0.152	0.610	--	0.038	0.10	
	0.762	0.152	0.610	--	0.033 & 0.048	0.043 & 0.063	
SARGISON and PERCY (2009)	0.5	0.25	0.20	0.004 to 0.015	0.06 to 0.14	0.12 to 0.28	Vertical wall.
				0.005 to 0.016	0.06 to 0.14	0.13 to 0.28	1H:1V upstream wall
				0.005 to 0.018	0.07 to 0.13	0.13 to 0.3	2H:1V upstream wall
Rounded-edged weir							
BAZIN (1896)	0.90	0.75	2.0	--	0.054 to 0.402	0.06 to 0.446	R = 0.10 m. Sér. 116.
	2.09	0.75	2.0	--	0.048 to 0.407	0.023 to 0.195	R = 0.10 m. Sér. 117.
WOODBURN (1932)	3.05	0.533	0.6096		0.1524 to 0.457	0.05 to 0.2	R = 0.051 to 0.203 m.
VIERHOUT (1973)	0.40	0.25	0.50	0.025 to 0.070	--	0.24 to 0.48	R = 0.10 m.
	1.20	0.25	0.50	0.065 to 0.100	--	0.155 to 0.202	R = 0.10 m.
ISAACS (1981)	0.42	0.0646	0.25	0.001-0.07	0.015 to 0.0675	0.036 to 0.161	
GONZALEZ & CHANSON (2007)							
Geometry 1	0.60	0.90	1.0	0.046 to 0.182	0.09 to 0.225	0.15 to 0.375	R = 0.057 m. Vertical upstream wall.
Geometry 2	0.88	0.90	1.0	0.05 to 0.26	0.096 to 0.29	0.10 to 0.32	R = 0.057 m. Vertical upstream wall.
Geometry 3	0.617	0.99	1.0	0.0064 to 0.17	0.023 to 0.21	0.037 to 0.337	R = 0.057 m. 0.25 m overhanging crest.
Geometry 4	0.617	0.99	1.0	0.0064 to 0.21	0.023 to 0.24	0.037 to 0.39	R = 0.057 m. Vertical upstream wall.
Small weir	0.42	0.0646	0.25	0.001 to 0.005	0.015 to 0.075	0.036 to 0.18	Vertical upstream wall.

Present study							
Large weir	1.01	1.0	0.52	0.0025 to 0.142	0.021 to 0.30	0.021 to 0.297	R = 0.080 m. Vertical upstream wall.
Small weir	0.42	0.0646	0.25	0.0012 to 0.0154	0.019 to 0.111	0.047 to 0.265	Vertical upstream wall.

Notes: H_1 upstream head above crest elevation; Q : water flow rate; R : radius of curvature; (--) : not available.

Fig. 1 - Definition sketch of a broad-crested weir

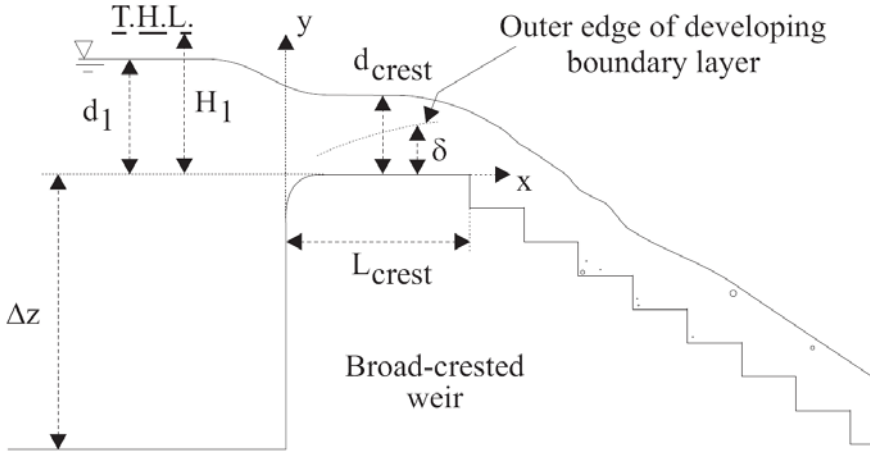

Fig. 2 - Dimensionless free-surface profiles above a broad-crested weir - Both point gauge (small squares & dashed line) and photographic (small crosses) data are presented, and the weir profile is shown in black - Note the distorted scale

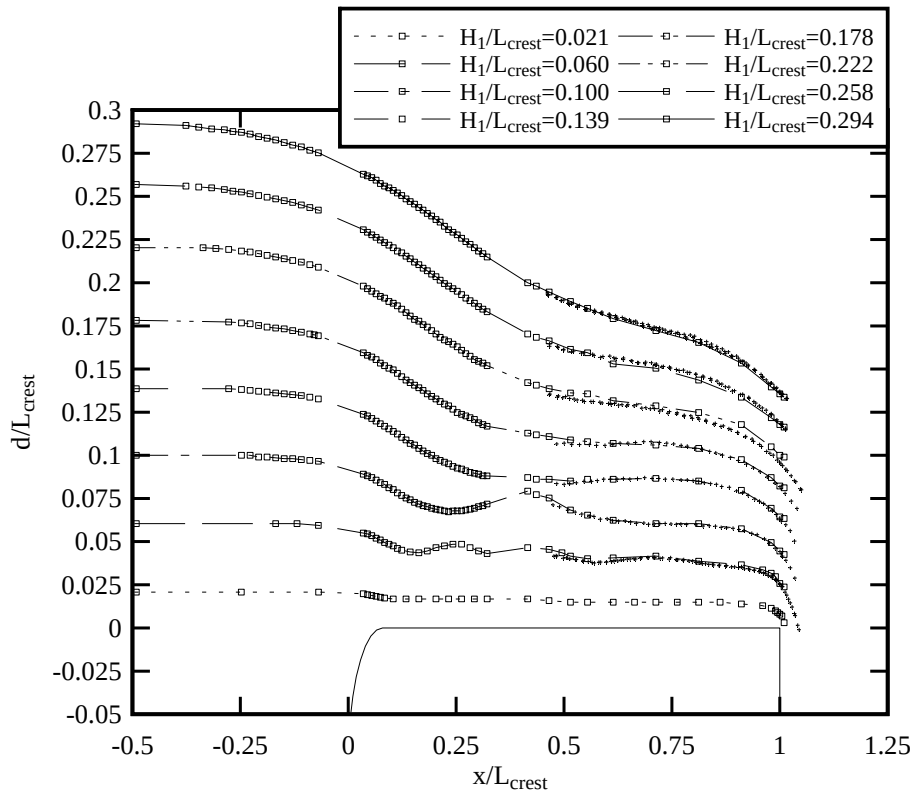

Fig. 3 - Dimensionless flow depth above the weir crest $d \times \Lambda / H_1$ as a function of $\beta \times C_D^2 \times \Lambda^2$ - Comparison between broad-crested weir data (Present study, $0.1 < x/L_{crest} < 1$), analytical solutions

(Eq. (5)), circular crested weir data (FAWER 1937, VO 1992) and undular flow data (CHANSON 2005)

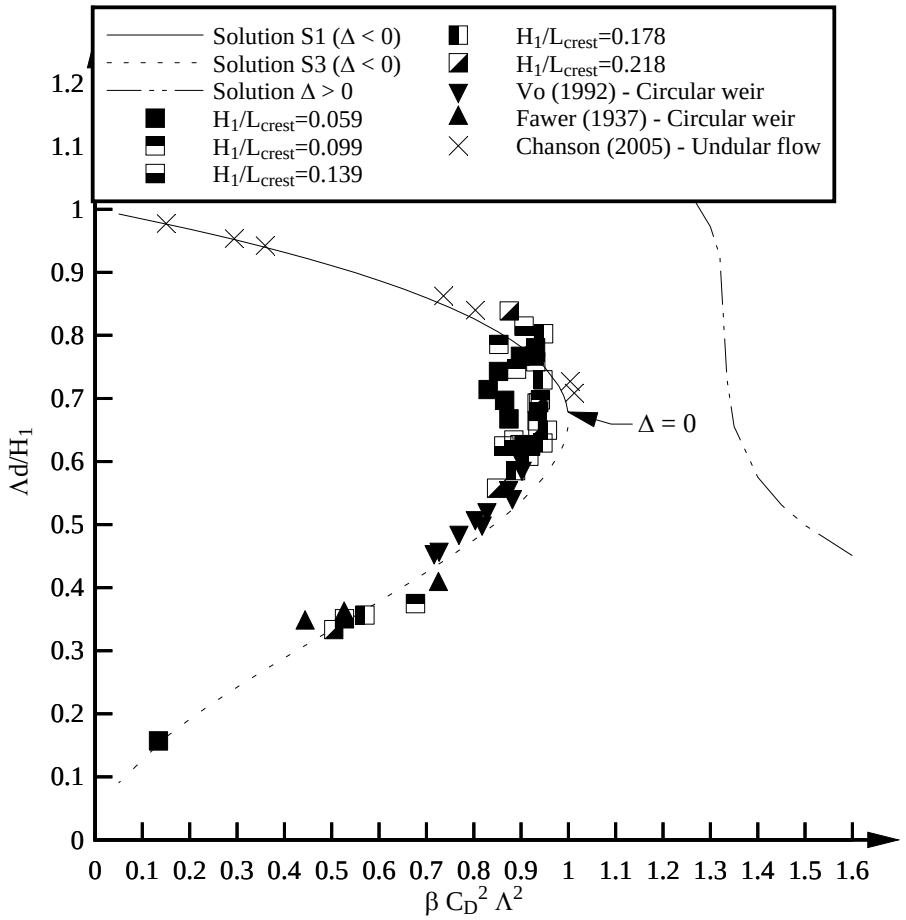

FELDER, S, and CHANSON, H. (2012). "Free-surface Profiles, Velocity and Pressure Distributions on a Broad-Crested Weir: a Physical study." *Journal of Irrigation and Drainage Engineering*, ASCE, Vol. 138, No. 12, pp. 1068–1074 (DOI: 10.1061/(ASCE)IR.1943-4774.0000515) (ISSN 0733-9437).

Fig. 4 - Dimensionless distributions of velocity and pressure along the broad-crested weir

(A) Velocity distributions for H_1/L_{crest} = 0.139

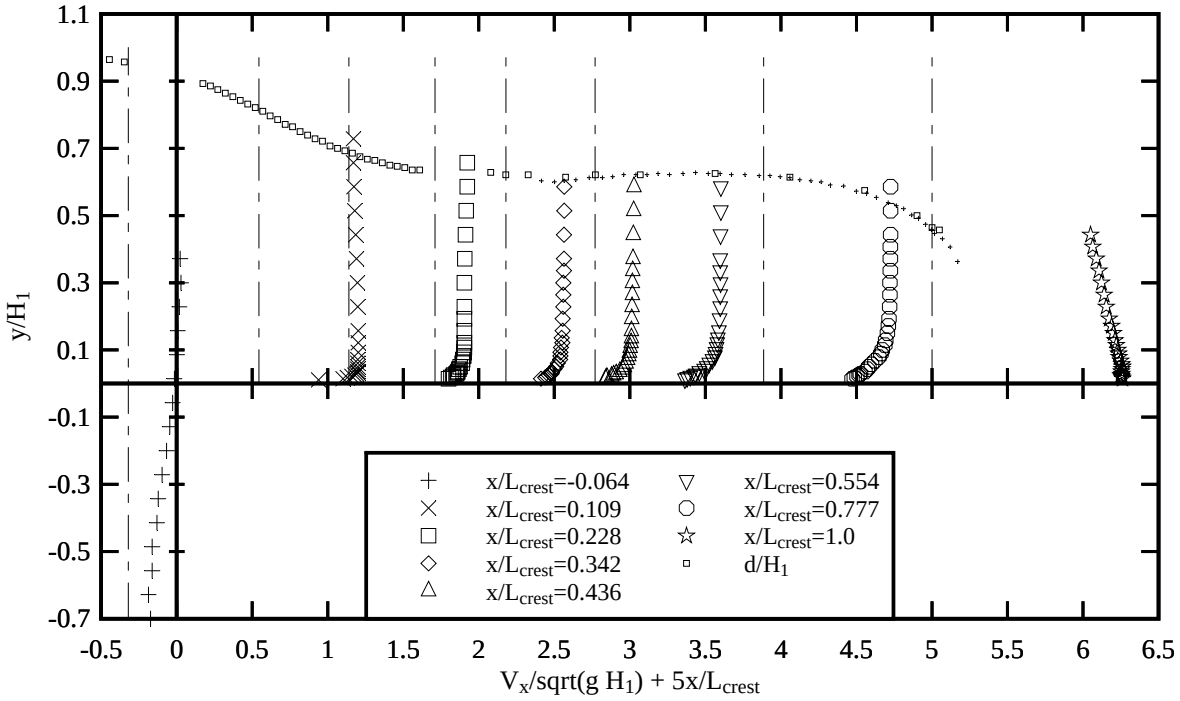

(B) Velocity distributions for H_1/L_{crest} = 0.224

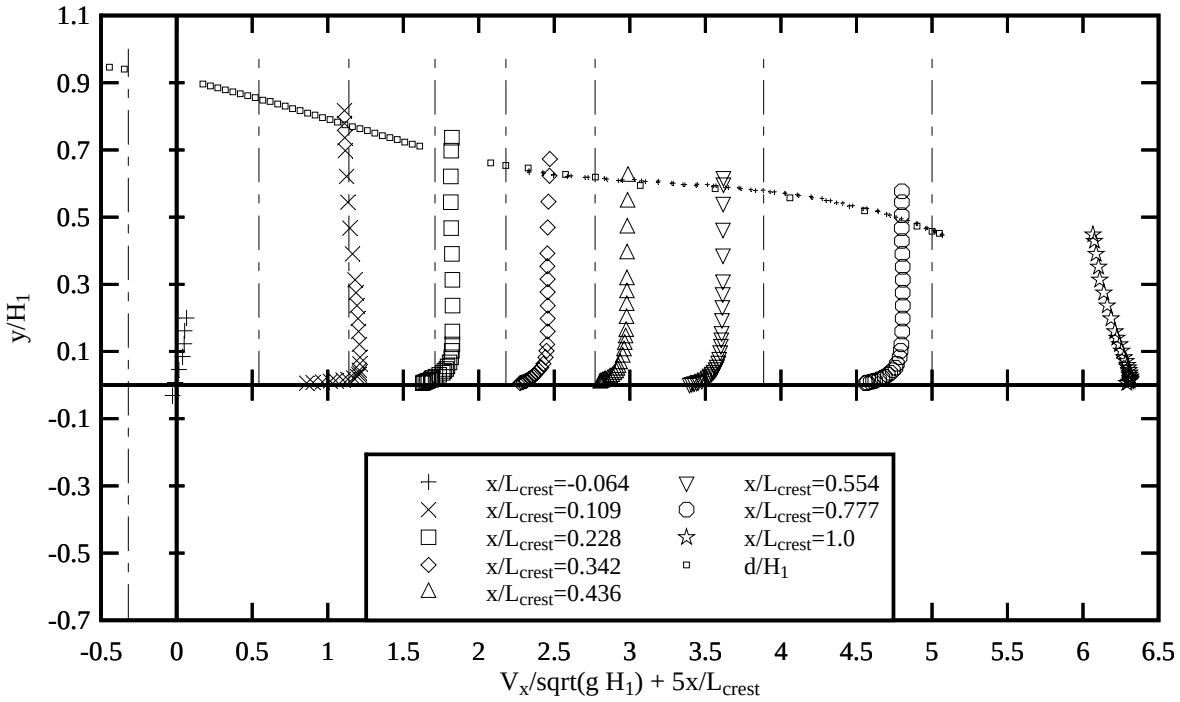

(C) Pressure distributions for H_1/L_{crest} = 0.224 - Comparison with the hydrostatic pressure and a Boussinesq equation solution for x/L_{crest} = 0.109 & 0.777

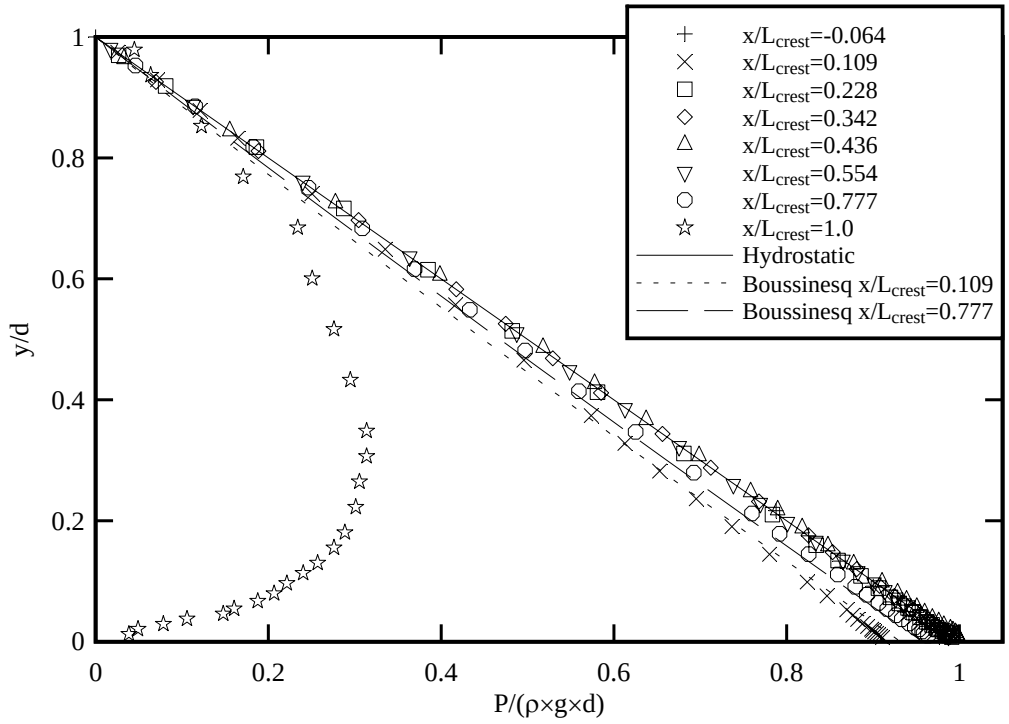

Fig. 5 - Dimensionless boundary layer thickness δ/H_1 - Comparison with the smooth boundary layer theory for H_1/L_{crest} = 0.099 & 0.178

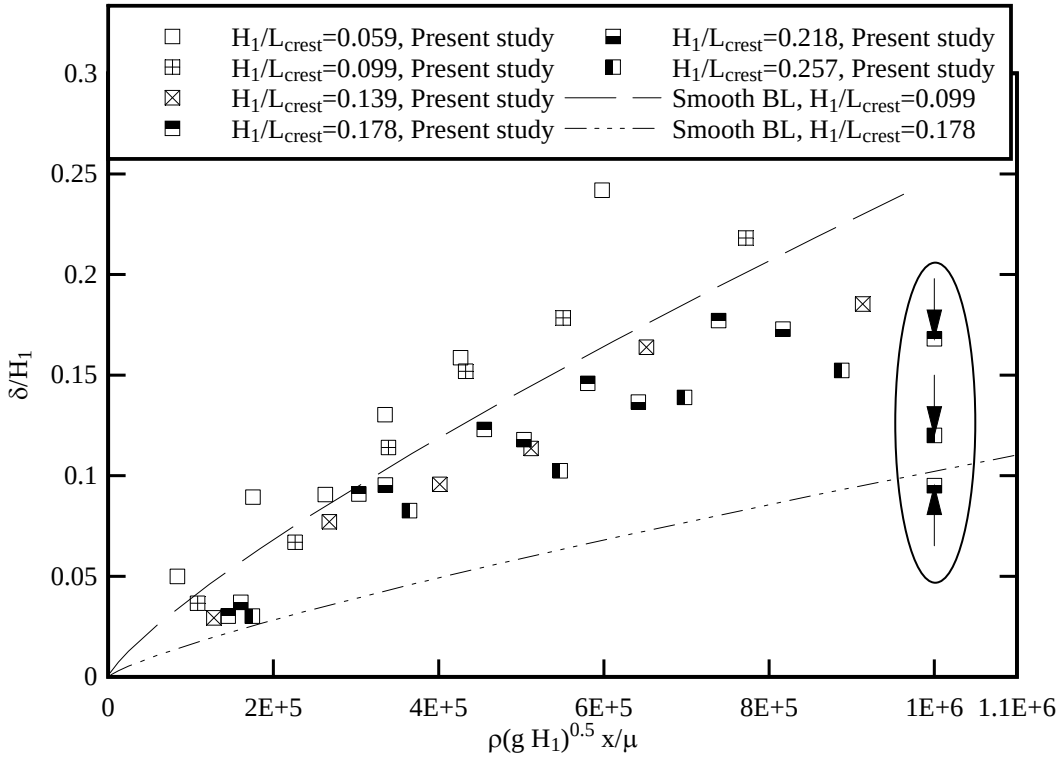

FELDER, S, and CHANSON, H. (2012). "Free-surface Profiles, Velocity and Pressure Distributions on a Broad-Crested Weir: a Physical study." *Journal of Irrigation and Drainage Engineering*, ASCE, Vol. 138, No. 12, pp. 1068–1074 (DOI: 10.1061/(ASCE)IR.1943-4774.0000515) (ISSN 0733-9437).

Fig. 6 - Dimensionless boundary shear stress $\tau_o/(\rho \times g \times H_1)$ above the crest - Comparison between logarithmic law and momentum integral equation results and the data of VIERHOUT (1973) obtained with a Preston tube

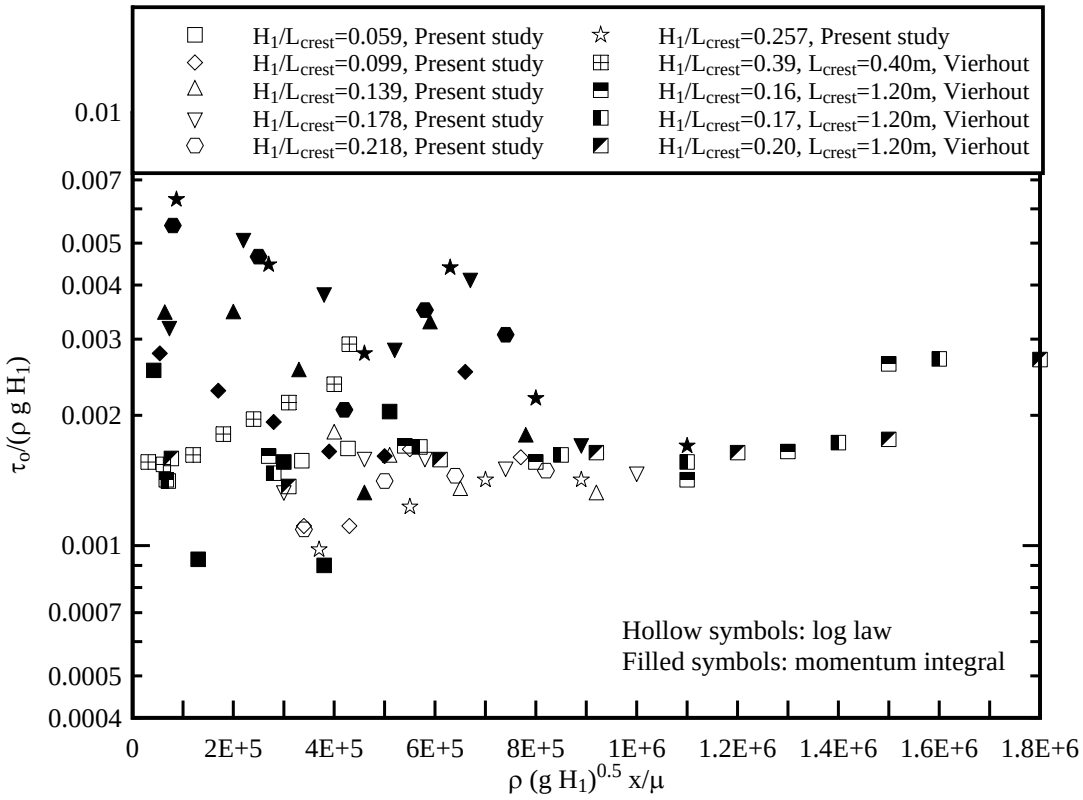

Fig. 7 - Dimensionless discharge coefficients for broad-crested weirs - Comparison with Equation (12), and previous studies with square-edge (BAZIN 1896, SARGISON and PERCY 2009), rounded edge (BAZIN 1896, VIERHOUT 1973, GONZALEZ and CHANSON 2007) and inclined upstream wall (SARGISON and PERCY 2009)